Scaling of intrinsic noise in an autocratic reaction network

Soutrick Das and Debashis Barik*
School of Chemistry, University of Hyderabad, Gachibowli, 500046, Hyderabad, India

(Received 4 December 2020; revised 10 February 2021; accepted 16 March 2021; published 7 April 2021)

Biochemical reactions in living cells often produce stochastic trajectories due to the fluctuations of the finite number of the macromolecular species present inside the cell. A significant number of computational and theoretical studies have previously investigated stochasticity in small regulatory networks to understand its origin and regulation. At the systems level regulatory networks have been determined to be hierarchical resembling social networks. In order to determine the stochasticity in networks with hierarchical architecture, here we computationally investigated intrinsic noise in an autocratic reaction network in which only the upstream regulators regulate the downstream regulators. We studied the effects of the qualitative and quantitative nature of regulatory interactions on the stochasticity in the network. We established an unconventional scaling of noise with average abundance in which the noise passes through a minimum indicating that the network can be noisy both in the low and high abundance regimes. We determined that the bursty kinetics of the trajectories are responsible for such scaling. The scaling of noise remains intact for a mixed network that includes democratic subnetworks within the autocratic network.

DOI: 10.1103/PhysRevE.103.042403

I. INTRODUCTION

Physiological functions of a living cell are controlled by networks of biochemical reactions. The complex reaction networks act as information processing machinery such that the cell can respond to various internal and external cues. In order to maintain the fidelity of diverse cellular responses, the machinery must perform reliably and robustly. However chemical reactions inside a cell often involve a finite number of macromolecular species and their fluctuations cannot be ruled out. The inherent probabilistic nature of the chemical reactions with a finite number of molecular species leads to stochastic trajectories of chemical reactions inside a living cell. The gene expression noise is the classic example of the finite number effect of chemical reactions [1–4] and is responsible for population heterogeneity of various cellular properties such as cell cycle [5] and cell signaling [6–9] in a homogeneous population of cells under uniform condition. The finite number effect is inherent to chemical reactions [10,11] and it can have beneficial effects to the organism in the context of adaptation [12,13] and innate immune response against pathogens [14]. The phenotypic diversity originating from the intrinsic noise allows single cell organisms to thrive in under unfavorable environmental conditions [15–17].

The chemical master equation approach and application of linear noise approximation on the chemical master equation allowed calculation of steady state moments of the protein and mRNA in the gene expression models [18–24]. These models explored the dependence of gene expression noise on various rate parameters that were found to be critical in controlling the transcriptional and translational bursts [25]. More recent studies have explored the epigenetic regulations of gene expression noise where the nucleosome positioning [26–29], TATA box binding affinity [30,31], and transcription factor binding sites [32–36] have been investigated further in the prokaryotic and eukaryotic systems. Subsequent modeling studies unraveled the roles of feedback regulations, positive and negative, in controlling noise in the functional regulatory networks [37–48].

Although a large number of modeling works have been carried out to elucidate chemical noise in small networks, however very little effort have gone into understanding noise regulation in large scale networks as a function of global architecture. Particularly, recent efforts towards determining the global organization of regulatory networks in prokaryotic and eukaryotic systems uncovered the hierarchical organization of these networks [49–54]. These studies have shown that the transcription factors are organized in a hierarchical fashion where multiple regulators are present in each hierarchy. In a hierarchal organization the transcription factors are organized in a layered fashion. The transcription factors in a particular layer regulate the transcription factors in other layers and in addition they may also interact with other transcription factors in the same layer. Furthermore, there seems to exist a common principle of organization for the regulators in terms of their abundance, lifetime, and variability [51]. These studies highlighted the existence of both pyramidal [50] and nonpyramidal [51] architectures of the networks. Furthermore, such hierarchical networks were also found to be present in the protein interaction network such as the kinase-phosphatase network in yeast [54]. The global structure of these networks have a remarkable resemblance to the social networks exhibiting autocratic, democratic, and a mixture of autocratic and democratic organization [53]. In an autocratic network a set of master genes dictate the regulation of a large number of

*dbariksc@uohyd.ac.in

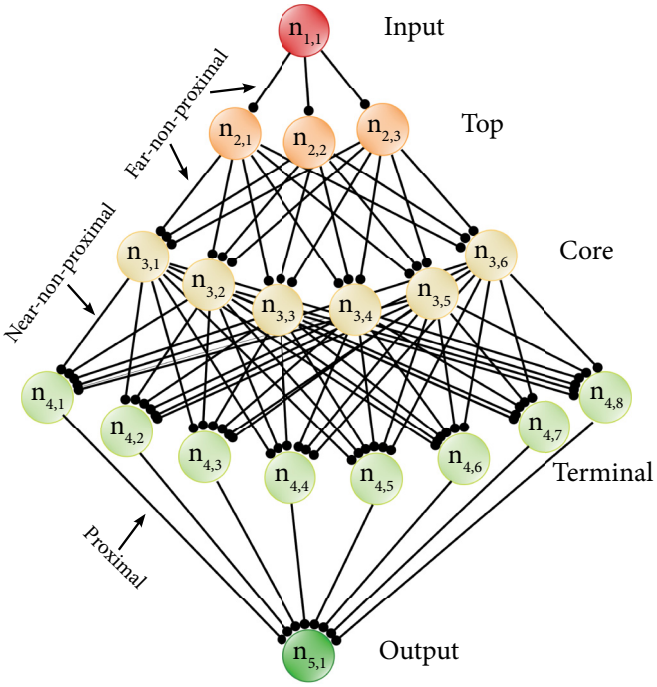

FIG. 1. Schematic representation of the autocratic network.

downstream genes through one or multiple layers of intermediate genes. Whereas in a democratic network the genes mutually interact with each other in response to external stimuli.

In this work we have investigated the regulation of intrinsic noise in an autocratic reaction network consisting of an input and an output node connected by three layers of nodes in between (Fig. 1). The nodes in the autocratic network are connected either by activatory or inhibitory regulatory interactions where a node regulates the expression of a node in the layer below resulting in unidirectional flow of information. Based on the proximity of the regulatory interactions, the direct and indirect regulations on the output node were categorized as proximal and nonproximal regulations, respectively. Nonproximal regulations via only one and more than one intermediate nodes were termed as near-nonproximal and far-nonproximal regulations, respectively. Our objective in this work was to determine the regulation of intrinsic chemical noise in the output node by the qualitative and quantitative nature of the proximal and nonproximal regulatory interactions. We systematically investigated the variation of average and noise in the output node with a varying number and the nature of the proximal and nonproximal interactions on it. We find that both the proximal and near-nonproximal interactions strongly influence the average abundance of the output node. The scaling of noise in the output node with the average strongly depends on the near-nonproximal interaction as compared to far-nonproximal interactions. Most importantly we uncovered an unconventional scaling of noise with the average abundance where the noise passes through a minimum indicating that even with high abundance the system can be significantly noisy. We determined that such behavior was due to the bursty nature of the trajectories that occur due to the increased number or strength of activatory proximal interactions. We further show that introduction of democratic interactions among the nodes in a particular hierarchy does not alter the scaling.

II. MODEL

In an autocratic network information flows only in one direction and there are no feedback regulations in the network. The network presented in Fig. 1 consists of nodes arranged in layers (or hierarchy) where nodes in a particular layer regulate the nodes in the adjacent layer of the lower level. The nodes in the lower level do not influence the nodes in the upper level and the nodes in a particular layer are noninteracting with each other. We termed the node at the highest and lowest levels as the input and output nodes, respectively. The three layers of nodes between the input and output nodes are denoted as the top, core, and terminal layer. The number of nodes in each layer, N_i, can be varied to create networks of different sizes ($d_N = \sum_i N_i$). These nodes generally are representative of chemical species that include genes, proteins, transcripts, or metabolites present inside a living cell. The regulatory influence from one node to the other is denoted by the lines with a circle on the receiving end and in an autocratic network all these circles point towards the same direction. Here the total number of interactions on the jth node in the ith layer ($m_{i,j}$) is given by the total number of nodes present in the layer above it ($m_{i,j} = N_{i-1}$). Furthermore, as the regulatory interaction could be either inhibitory or activatory, we varied the number of inhibitory ($m^-_{i,j}$) and activatory ($m^+_{i,j}$) interactions, with the conservation relation $m^-_{i,j} + m^+_{i,j} = m_{i,j}$, to study the effect of these interactions on the chemical noise in the network. We define the total number of the inhibitory regulations across all nodes in a particular layer as $M^-_i = \sum_j m^-_{i,j}$. A similar definition also holds for the activatory interactions. In addition to the regulatory influence, each node also has its unregulated production and degradation/dilution reactions. In this work we have chosen the following number of nodes $N_1 = 1, N_1 = 3, N_3 = 6, N_4 = 8$, and $N_5 = 1$ in the input, top, core, terminal, and output layers, respectively. Consequently the number of regulatory interactions on each node in the top, core, terminal, and output layer are given as 1, 3, 6, and 8, respectively. We define the mean field dynamics of the nodes by a set of coupled ordinary differential equations as

$$\frac{d\overline{n}_{i,j}}{dt} = \Omega\kappa_{i,j} - \gamma_{i,j}\overline{n}_{i,j} + \frac{1}{\Omega}\sum_{k=1}^{N_{i-1}} a_{i,k}\overline{n}_{i-1,k}\overline{n}_{i,j}. \qquad (1)$$

The equation represents the time evolution of the average molecular abundance ($\overline{n}_{i,j}$) of the jth node in the ith layer. The first two terms represent gain and loss due to production and degradation/dilution, respectively. $\kappa_{i,j}$ and $\gamma_{i,j}$ are the associated rate constants with these two reactions. The last term represents the bimolecular regulatory interaction from the kth node in the $(i-1)$th layer. The strength and the nature of the regulation are determined by the value and the sign of $a_{i,k}$, respectively. $a_{i,k} < 0$ and $a_{i,k} > 0$ represent inhibitory and activatory regulations, respectively. The number of inhibitory and activatory interactions on the jth node are determined by $m^-_{i,j}$ and $m^+_{i,j}$. In the autocratic network there are a total $M = \sum_{i=2} N_{i-1}N_i$ number of regulatory interactions shared

across d_N number of nodes. Throughout this work we have kept a fixed value of $k_{i,j} = 0.012$ and $\gamma_{i,j} = 0.02$ for the production and the degradation rate constants, respectively. The strengths of the activatory and inhibitory regulations were denoted by a^+ and a^- and were chosen to be equal to ± 0.003, respectively. We chose these parameter sets considering that the number of molecules per node must be in the realistic range that is commonly found in a live cell and the system must reach a stationary state in a finite simulation time. Note that we have not specifically mentioned the units of the rate constants, particularly for the time, to make the model applicable to networks corresponding to different organisms as timescales can be significantly different from one organism to another. However, the chosen value of the degradation constant $\gamma_{i,j}$ represents a half-life of ∼35 time units which is the most common half-life for many proteins in budding yeast [55] (in min) and in mammalian [56] (in hour) systems. Ω is the scaling factor that scales the population abundance of the interacting nodes keeping the dynamics of the system unchanged. Unless specifically mentioned, throughout the paper we have used $\Omega = 100$.

We determined the effect of finite numbers in the autocratic networks by simulating the chemical reactions corresponding to the model (1) using Gillespie's stochastic simulation algorithm [57]. The linearity of the reaction rate laws in the model allowed us to accurately estimate the effect of intrinsic noise. In an autocratic network of size d_N, there are $2d_N + M$ number of reactions involved corresponding to d_N production, d_N degradation, and M regulatory interaction (M). In order to obtain accurate steady state statistics, we ran an ensemble of 10 000 trajectories for a long time (50 000 time units). The runtime of stochastic simulation can be extremely long when the propensity of the chemical reactions becomes large due to the involvement of the large number of molecular species and/or large rate constants of the chemical reactions. In order to avoid a very large runtime of the stochastic calculations we implemented a cutoff rule of 100 000 molecules/node to stop the calculation which becomes significantly slower with large population abundance. We do not include this calculation in the analysis. This choice of cut-off rule is not completely unreasonable due to the fact that the finite number effect will be extremely small with the large abundance.

III. RESULTS

We first determined the dependence of average abundance of the output node on the number of proximal and nonproximal regulations. The proximal interactions are direct regulatory interactions from the nodes in the terminal layer to the output node (Fig. 1), whereas the nonproximal interactions are regulations that indirectly influence the output node and they are the interactions between the nodes in the input/top, top/core, and core/terminal layers. Here we categorized the nonproximal interactions into two groups as near-nonproximal and far-nonproximal interactions. The regulations on the terminal layer are termed as the near-nonproximal group and the regulations on the core and top layer are termed collectively as the far-nonproximal group. The average abundance of the output node ($\overline{n}_{5,1}$) decreases with the increasing number of proximal inhibitory interactions (m_p^-) for a fixed number of inhibitory near-nonproximal ($m_{\rm nnp}^- = \sum_{j=1}^{N_4} m_{4,j}^-$) and far-nonproximal interactions ($m_{\rm fnp}^- = \sum_{j=1}^{N_2} m_{2,j}^- + \sum_{j=1}^{N_3} m_{3,j}^-$) on the nodes in various layers (Fig. 2). We increased the number of inhibitory regulations on each node in the terminal layer $m_{4,j}^-$ by 1 to increase $m_{\rm nnp}^-$. For the ease of implementation we have followed a specific order to assign the inhibitory interactions on a particular node in the terminal layer from the nodes in the core layer. Specifically the inhibitory interactions originate from the nodes on the left of the core layer. For example, for $m_{4,j}^- = 1$ ($m_{\rm nnp}^- = 8$), the node $n_{3,1}$ inhibits all the nodes in the terminal layer and for $m_{4,j}^- = 2$ ($m_{\rm nnp}^- = 16$), the nodes $n_{3,1}$ and $n_{3,2}$ inhibit all the nodes in the terminal layer. We adopt the similar strategy to change $m_{\rm fnp}^-$. With an increasing number of $m_{\rm nnp}^-$ the value of $\overline{n}_{5,1}$ decreases across different values of m_p^- (Fig. 2). However when the proximal inhibitory regulations are proportionately more than activatory regulations ($m_p^- > 4$) an increased number of near-nonproximal inhibitory regulations help increase the abundance of the output node. Therefore both the proximal and near-nonproximal interactions regulate the abundance of the output node. Now, in order to determine how the far-nonproximal interactions in the top and core layer regulate the abundance of the output node, we plotted $\overline{n}_{5,1}$ vs m_p^- for different numbers of $m_{\rm fnp}^-$ for a fixed number of $m_{\rm nnp}^-$ (Fig. 3). The effect of the far-nonproximal inhibitory interactions on the output node is quite small across different values of $m_{\rm nnp}^-$. Therefore in an autocratic network proximity of the regulatory interactions are important in dictating the extent of regulation.

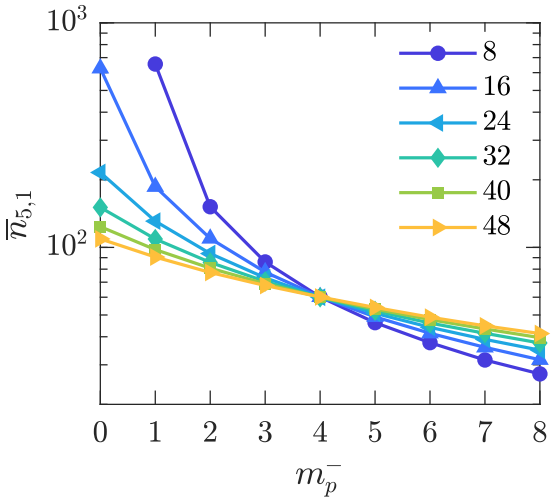

FIG. 2. Plot of the average abundance of output node ($\overline{n}_{5,1}$) as a function of the number of inhibitory proximal interactions on the output node (m_p^-) for the indicated number of inhibitory near-nonproximal interactions ($m_{\rm nnp}^-$) on the nodes in the terminal layer. The value of $m_{\rm fnp}^-$ was kept fixed at 6. The data represent the average of three independent runs and the sizes of the error bars of $\overline{n}_{5,1}$ are similar or smaller than the sizes of the markers.

The scaling of the noise, measured by the coefficient of variation (CV) with the average abundance, is an important aspect of noise regulation in biochemical reaction networks. In Fig. 4(a) we plot CV of the output node at the steady state with the average abundance obtained by varying the

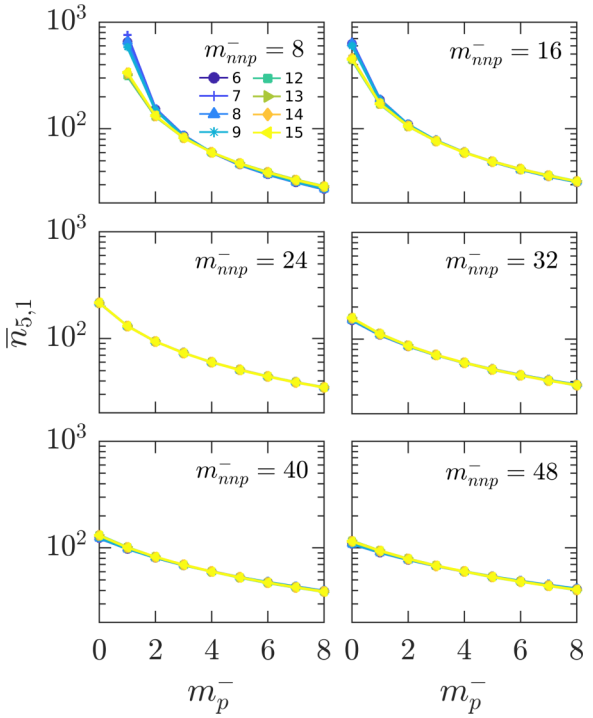

FIG. 3. Plot of $\overline{n}_{5,1}$ with m^-_p for a different number of far-nonproximal inhibitory interactions with a particular value of m^-_{nnp}. Each line type corresponds to a particular value of m^-_{fnp} as indicated in the figure.

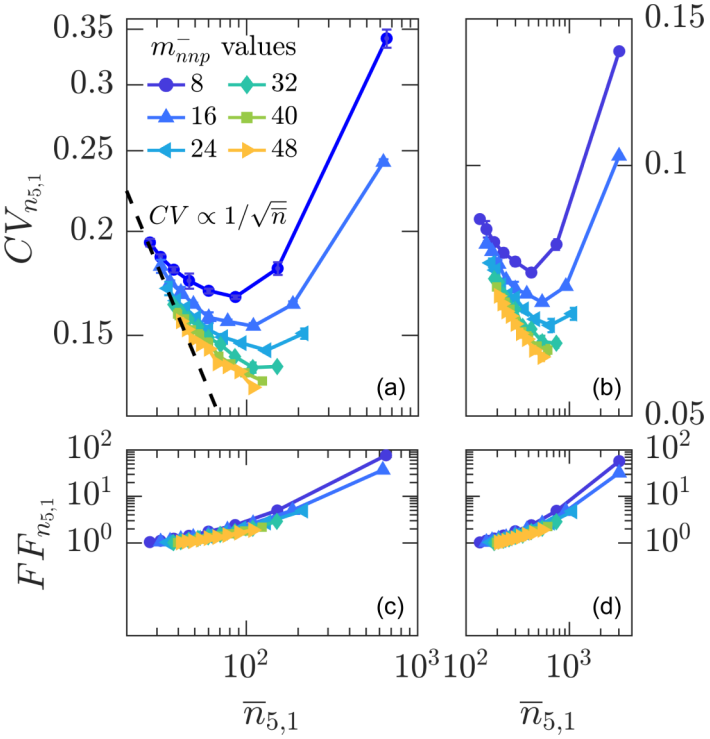

FIG. 4. (a) Plot of the CV of output node ($\text{CV} = \sigma/\overline{n}$, $\sigma =$ standard deviation) with the $\overline{n}_{5,1}$ for different values of m^-_{nnp} with a fixed value of $m^-_{\text{fnp}} = 6$. The dashed line corresponds to $1/\sqrt{\overline{n}}$ scaling of the CV. (b) CV vs $\overline{n}_{5,1}$ plot for the network with 5× increased abundance ($\Omega = 500$). The different color/line type are for different values of m^-_{nnp}. The plot of Fano factor ($\text{FF} = \sigma^2/\overline{n}$) with the average for low (c) and high (d) abundance regimes. Note that m^-_p was varied to achieve the different values of average abundance in the output node.

number of proximal inhibitory interactions (m^-_p). We find that the qualitative behavior of the scaling of noise with the average depends critically on the near-nonproximal interactions. For the larger values of m^-_{nnp} the noise decreases with the average—an expected behavior of the finite number effect. However, for the smaller values of m^-_{nnp}, with increasing average the CV initially decreases and passing through a minimum it increases further [Fig. 4(a)]. The decrease of noise with the increasing abundance is expected based on the finite number effect of the stochastic chemical kinetics. However, the increase of noise with increasing average is nonintuitive in nature and therefore a nontrivial or unconventional outcome of the system. In order to determine the generality of the scaling behavior that is independent of a particular range of abundance, we repeated these calculations by scaling all the rate constants systematically such that the abundance of all the nodes increase in a consistent manner ($\Omega = 500$). In Fig. 4(b) we show the scaling of the noise with the average abundance where the rate constants were scaled to achieve higher average abundance. We find qualitatively similar scaling behavior of the noise as was in Fig. 4(a) with $\Omega = 100$. Note that the values of CV are now smaller and the turning point of the CV occurs at the higher average abundance. Therefore these results indicate that the unconventional scaling is an intrinsic property of the autocratic network and it depends on the number of inhibitory regulations on the terminal layer (m^-_{nnp}). The comparison of the CV for the different values of m^-_{nnp} also highlight that a large number of inhibitory regulations on the upstream layer reduces the variability in the output node. The plots of Fano factor (FF) with the average [Figs. 4(c) and 4(d)] indicate that the strength of the noise increases with the decreasing number of proximal inhibitory regulations. Thus the direct activatory regulations are responsible for increasing the amplitude of the intrinsic noise. We next determined the effect of the far-nonproximal interactions on the scaling of noise. We find that at a particular value of m^-_{nnp} the scaling of noise is mostly independent of the number of far-nonproximal inhibitory interactions (Fig. 5). Therefore the qualitative nature of the scaling of noise in the output node is dictated by the near-nonproximal interactions on the terminal layer and is independent of the far-nonproximal interactions originating at the top and core layers.

The surprising aspect of the stochasticity in the autocratic network is the increase of variability with increased abundance. As the steady state distribution cannot split in this network due to the lack of feedback regulation and nonlinearity, a possible way the network can exhibit higher noise in the high abundance regime is via change of the shape of the distribution. In Fig. 6(a) we plot the steady state distributions of the population abundance of the output node with an increasing number of proximal inhibitory interactions for a fixed value of m^-_{nnp} and m^-_{fnp}. These distributions clearly indicate that the increased noise is not due to the multimodality of the steady state distributions. Consistent with the CV, the widths

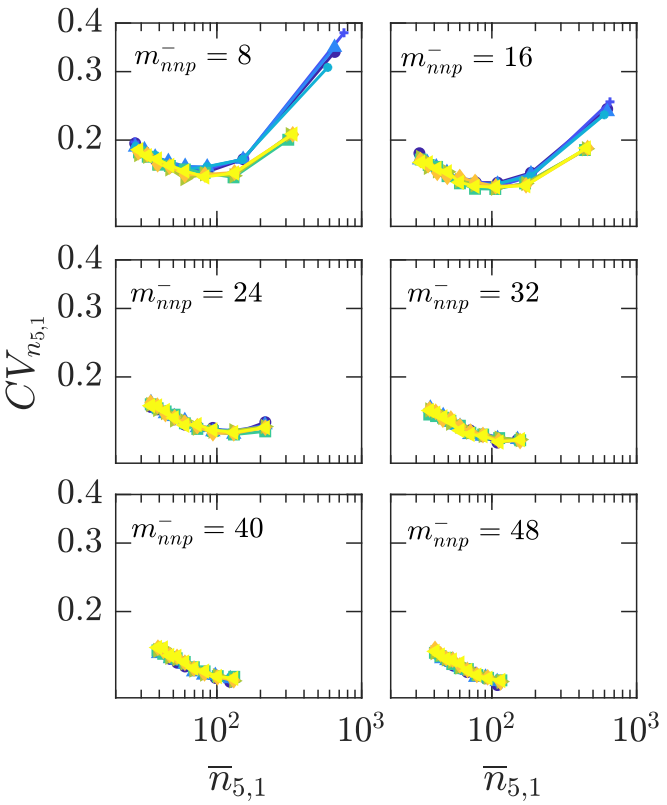

FIG. 5. CV vs $\overline{n}_{5,1}$ plot for different values of m^-_{fnp} with the indicated values of m^-_{nnp}. The different color/line type are for different values of m^-_{fnp} as indicated in Fig. 3.

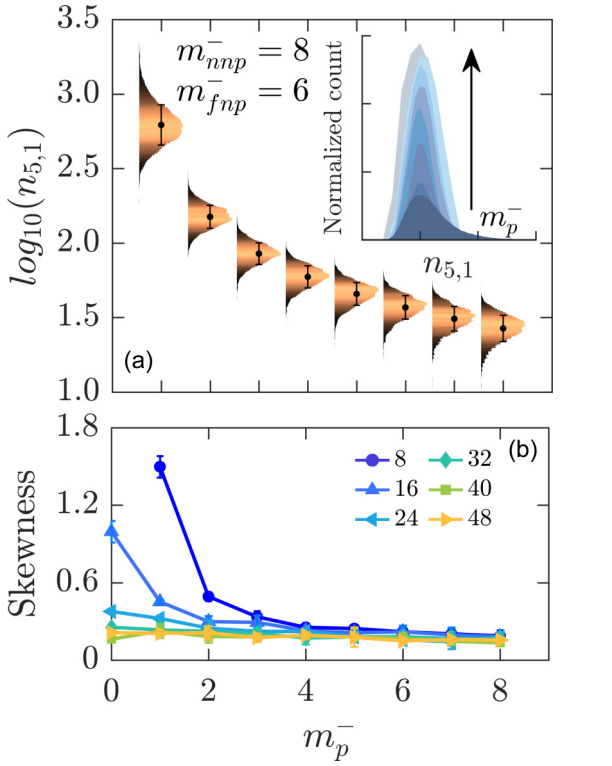

FIG. 6. (a) Plot of steady state population distribution of the output node for a different number of proximal inhibitory regulations. Comparison of distributions centered at the abundance corresponding to the peak of the distribution (inset). (b) Plot of skewness of the steady state population distributions as a function of m^-_p for the indicated value values of m^-_{nnp} and a fixed value of $m^-_{\text{fnp}} = 6$.

of the distributions in the high and low abundance regimes are higher as compared to the width in the intermediate region of the average. We further compared these distributions, centered at the peak, to determine the change in the shapes with m^-_p [Fig. 6(a) inset]. The distribution corresponding to a low value of m^-_p is significantly skewed towards a large value of $n_{5,1}$ (positively skewed) as compared to the high value of m^-_p. Furthermore, the plot of skewness vs m^-_p [Fig. 6(b)] clearly shows that the increased variability in the output node is due to the large and rare fluctuations.

In order to find out the origin of such increased variability, we then looked at the trajectories of the output node for different values of m^-_p (Fig. 7). In the large abundance limit with $m^-_p = 1$, the stochastic trajectory exhibits a fluctuation pattern reminiscent of bursty gene expression kinetics. Particularly, the large and infrequent fluctuations make the system significantly noisy and the steady state distribution becomes positively skewed. Whereas in the low abundance limit with larger values of m^-_p, the stochasticity in the time courses seems to be regular and devoid of any large deviations from average. We further plot the phase space of the system by plotting the time course of the output node against the time course of a representative node in the terminal layer (Fig. 7). The phase space plot for $m^-_p = 1$ indicates the bursty nature of the output node as it covered a larger area in the phase space as compared to the phase space for the larger values of m^-_p. With $m^-_p = 1$ the output node receives only one inhibitory and seven activatory input signals from the nodes in the terminal layer. Due to the larger number of activatory signals, the production of the output node is accelerated which cannot be compensated by the small number of inhibitory interactions. The ultimate result of these two opposing interactions is reflected in the form of bursty kinetics of the output node. The excitable nature of the output node disappears with an increasing number of the inhibitory input signals that counters the production by accelerating degradation of the output node.

The variation of m^-_p changes the average abundance on the output node due to increased inhibitory regulation from the nodes in the terminal layer to the output node. Therefore, in order to keep the average abundance unchanged, we increased the synthesis rate ($k_{5,1}$) while we changed m^-_p. Under this condition, the average remained the same while we varied m^-_p (inset of Fig. 8). The noise in the output node was found to decrease with the increase of m^-_p keeping the average unchanged (Fig. 8). We found similar behavior across different values of m^-_{nnp}. However, the effect of m^-_p is prominent for smaller value of m^-_{nnp} similar to findings in Figs. 4(a) and 4(b). These results again indicate that a large number of activatory interactions (small m^-_p) on the output node contribute to increased variability. Therefore the high noise in the high abundance regime is a direct consequence of the increased number of activatory interactions on the output node.

So far we have kept the strengths of activatory and inhibitory regulations (a_+ and a_-) equal and varied the number

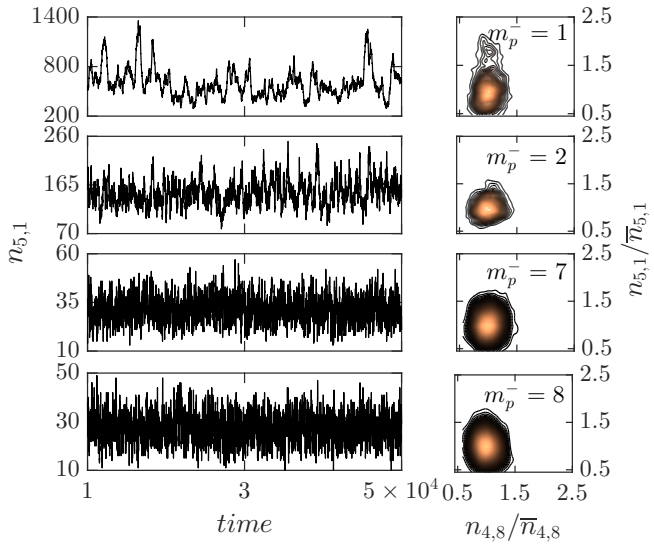

FIG. 7. The trajectories (left) and the phase space plots (right) of the network with $m^-_{\text{nnp}} = 8$ and $m^-_{\text{fnp}} = 6$. In the phase space plot the output node $n_{5,1}(t)$ is plotted as a function of $n_{4,8}(t)$, a node in the terminal layer.

of proximal and nonproximal interactions. We next varied the rate constants of the activatory and inhibitory interactions to determine the effect of the strengths of these interactions on the scaling of the intrinsic noise. We varied the ratio of these two rate constants by a factor of 2. In Figs. 9(a) and 9(b) we plot the scaling of the noise for $a_+/a_- = 2$ and $a_+/a_- = 0.5$, respectively. The nontrivial scaling of noise becomes more prominent across the different number of near-nonproximal interactions when the strengths of activatory interactions were more than the strengths of negative interactions [Fig. 9(a)]. Whereas for the higher strength of negative interactions [Fig. 9(b)], the network seems to exhibit usual scaling across a different number of near-nonproximal interactions. Further-

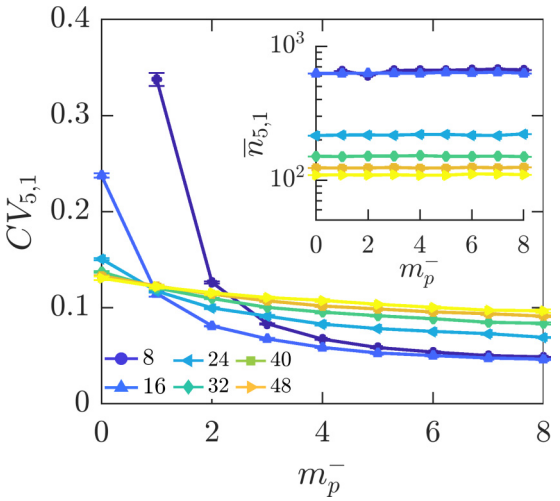

FIG. 8. Plot of CV vs m_p^- for $m^-_{\text{fnp}} = 6$ and different m^-_{nnp}. While modifying m_p^-, the synthesis rate of the output node $k_{5,1}$ was adjusted such that the average remains unchanged (inset). The different color/line type are for different values of m^-_{nnp} as indicated in Fig. 4.

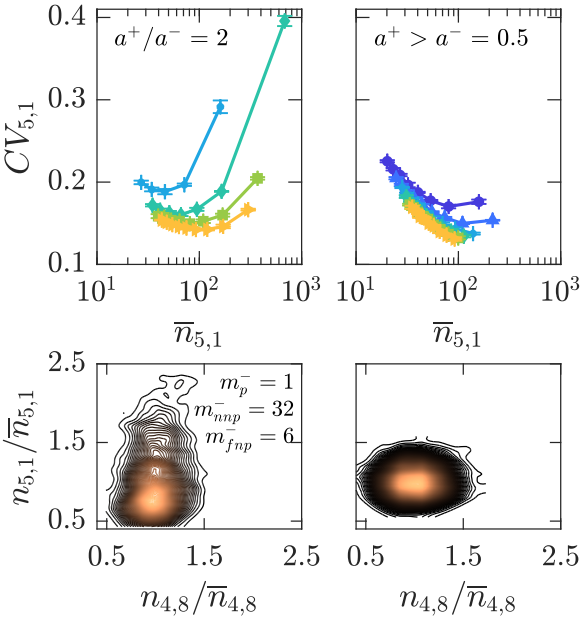

FIG. 9. CV vs average plots for the output node with $a^+ = 0.006$, $a^- = 0.003$ (a) and $a^+ = 0.003$, $a^- = 0.006$ (b). The phase space plots for these two conditions (c) and (d). The different color/line type are for different values of m^-_{nnp} as indicated in Fig. 4.

more, the phase space plots in these two cases indicate the bursty nature of the output node for $a_+/a_- = 2$ [Fig. 9(c)] as compared to $a_+/a_- = 0.5$ [Fig. 9(d)]. We showed in Fig. 7 that the bursty nature of the trajectory is responsible for amplifying the noise in the larger abundance limit. This argument of the bursty kinetics is further supported by the fact that the higher strength of positive interactions promote the nontrivial scaling of noise. Furthermore, we also looked at the scaling under the variation of interaction strengths at each layer. We performed calculations with different interaction strengths in each layer to determine the layer-specific regulatory role of the interaction strengths on the scaling of the noise. We carried out two sets of calculations where in one set we increased the strength of interaction from the input to the output layer [Fig. 10(a)] and in another set we decreased the interaction strength [Fig. 10(b)]. In the case of increasing strength from the input to the output layer, we have chosen the values of interactions as $a_{2,j} = \pm 0.003$, $a_{3,j} = \pm 0.004$, $a_{4,j} = \pm 0.005$, and $a_{5,j} = \pm 0.006$ for the interaction between input/top, top/core, core/terminal, and terminal/output layers, respectively. We used the reverse order for the decreasing strength of interactions from the input to the output layers. We find that in both cases the scaling of noise with the average are similar. However, across different values of m^-_{nnp} the high noise in the high abundance nature of noise is more prominent when the strength of interactions were larger in the terminal layer [Fig. 1(a)].

The autocratic network we have investigated is fully connected in a sense that every node in the network is connected to all the nodes in the layer above and below. However, in reality networks may not be fully connected [58]. Therefore to estimate the noise in such types of autocratic network, we randomly removed a certain fraction of regulatory interactions

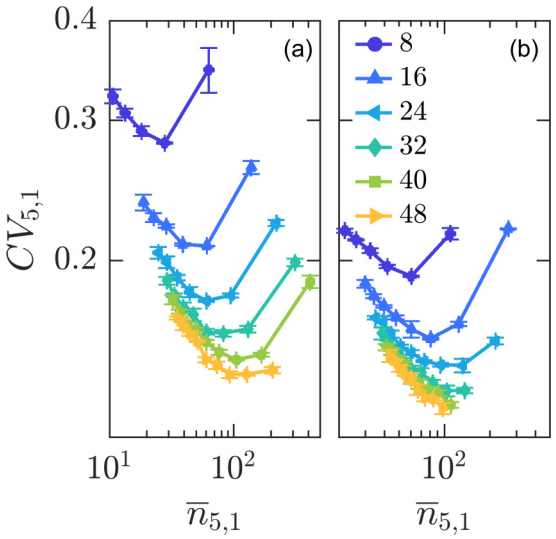

FIG. 10. CV vs average plots for the output node with an increasing order of interaction strength from top to bottom (a) and bottom to top (b) layer of the network. The different color/line type are for different values of $m^-_{\rm nnp}$ as indicated inside the plot.

from the network across all layers except the output layer. In order to remove a certain number of interactions from the top, core, and terminal layers of the network, we set the values of randomly selected $a_{i,j}$ to 0. For example, in order to remove ∼20% interactions, we set 1, 6, and 8 numbers of randomly selected $a_{i,j}$ from the top, core, and terminal layers, respectively. Note that in the fully connected network the total number of interactions is 69 in these three layers. We doubled these numbers in the case of ∼40%. We find that with the removal of ∼20% and ∼40% regulatory interactions from the network do not alter the scaling of the noise (Fig. 11) indicating the universality of the scaling behavior in the autocratic network.

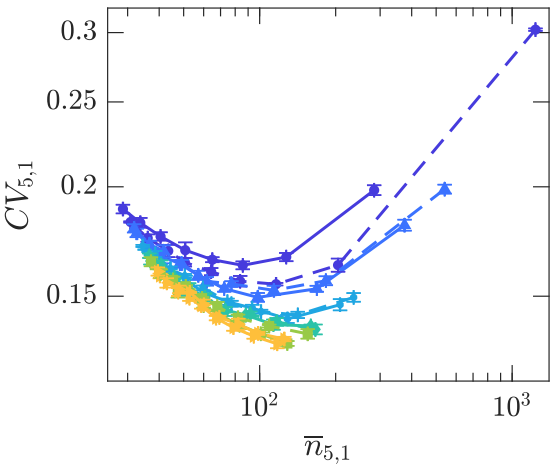

FIG. 11. Comparison of the scaling with ∼20% (solid lines) and ∼40% (dashed lines) reduction of the interactions, at random, in the top, core, and terminal layers of the network. The different color/line type are for different values of $m^-_{\rm nnp}$ as indicated in Fig. 4.

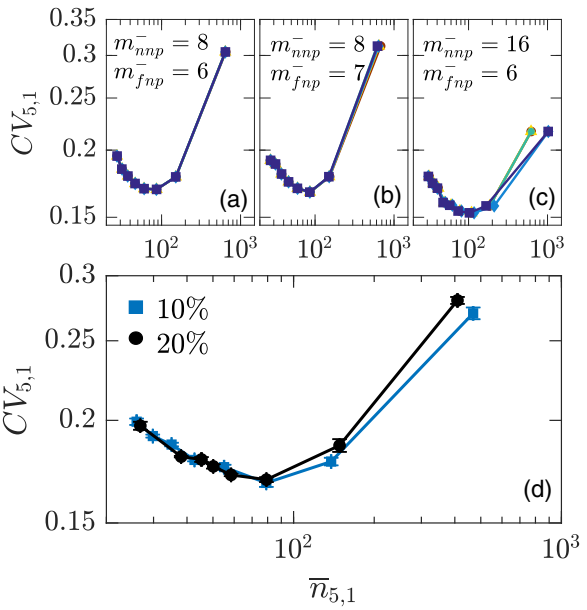

FIG. 12. (a)–(c) Scaling of noise in the output node with an average abundance for the indicated values of $m^-_{\rm nnp}$ and $m^-_{\rm fnp}$. For each combination of $m^-_{\rm nnp}$ and $m^-_{\rm fnp}$, plots for five different networks having randomly chosen mutual interactions are presented. (d) Scaling of noise for the networks ($m^-_{\rm nnp} = 8$ and $m^-_{\rm fnp} = 6$) with all the rate parameters distributed log-normally having 10% (square blue) and 20% (circle black) variation about the mean. The mean of these parameters are $\langle \kappa_{i,j} \rangle = 0.012$, $\langle \gamma_{i,j} \rangle = 0.02$, $\langle a^+ \rangle = 0.003$, and $\langle a^- \rangle = -0.003$.

In the autocratic network we have chosen the regulatory interactions in a specific manner to create a network with a certain number of inhibitory near-nonproximal and far-nonproximal interactions. However, different mutual combinations of interactions can satisfy a given number of $m^-_{\rm nnp}$ and $m^-_{\rm fnp}$ (macrostate), thereby creating many other possible equivalent networks (microstate). In order to determine whether our conclusions are dependent on the specific choice of the mutual interactions (i, j), we generated five equivalent networks with randomly selected mutual interactions all having the same values of $m^-_{\rm nnp}$ and $m^-_{\rm fnp}$. In Figs. 12(a)–12(c) we show that the qualitative nature of the scaling is independent of the specific choice of mutual interactions. Furthermore, the entire network is symmetric in a sense that the rate parameters are the same from one node to another. Therefore, in order to estimate the effect of variation of the parameters from one node to another, we calculated the scaling of noise for the asymmetric network where the rate parameters were sampled from log-normal distributions with the average values used for the symmetric network. We show that the scaling is independent of the variation of the parameters of the individual nodes [Fig. 12(d)].

Finally we determined the scaling of noise in a mixed network where the nodes in a particular hierarchy are connected with each other resulting in a democratic architecture within the hierarchy. Therefore the nodes in the top, core, and the terminal layer regulate each other forming a democratic subnetwork within themselves [59]. The resulting network therefore becomes a conglomeration of autocratic and demo-

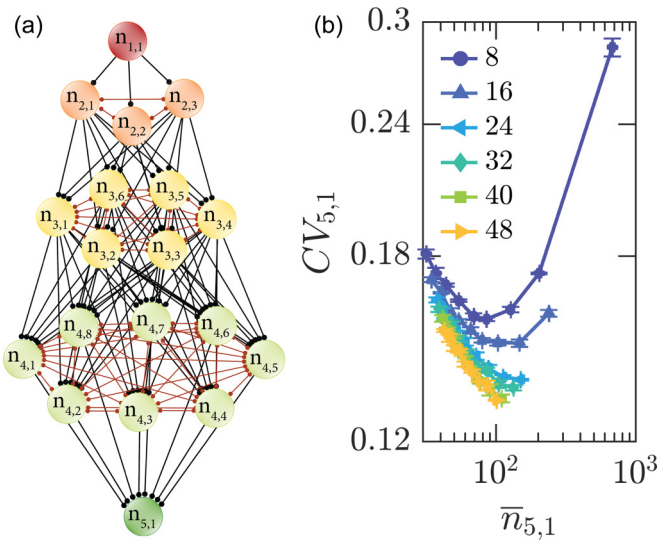

FIG. 13. (a) Schematic representation of the mixed network. The nodes in the top, core, and terminal layers form democratic subnetworks within themselves. The mutual interactions within a democratic subnetwork are represented by the edges with filled circles at both ends (red lines). (b) The scaling of noise in the output node with its average. The values of a^+ and a^- were chosen as $+0.0025$ and -0.0025, respectively. In the democratic subnetworks activatory and inhibitory interactions were equally distributed with a strength of 0.001 for both interactions.

cratic networks [Fig. 13(a)]. We find that the democratic mutual interactions in the three layers do not alter the scaling of intrinsic noise with the average [Fig. 13(b)]. Similar to the purely autocratic network, the mixed network also exhibits high noise both in the low and high abundance regimes.

IV. CONCLUSION

Population heterogeneity is an integral aspect of cellular physiology owing to the gene expression noise originating from the fluctuations of a finite number of molecular species inside a microscopic cell volume [10,11]. The cell-to-cell variability of various cellular attributes can have a detrimental effect on the survival and fitness of the organism in the altered environment conditions. Therefore understanding the means of regulating chemical noise is a crucial aspect. A large volume of work have investigated the various facets of gene expression noise modeled by the simple reaction schemes involving a gene, mRNA, and protein. These models have unearthed a wealth of information about the origin of observed variability in protein levels due to transcriptional and translational bursting [25]. Subsequent models investigated the role of network topology in regulating intrinsic noise in small regulatory motifs [18,20,25] and system level regulatory networks [60,61]. However, investigation of chemical noise in a network with global architecture is lacking. Particularly, recent studies established the global architecture of regulatory networks highlighting a hierarchical nature of system level networks with a close resemblance to the social networks such as democratic, autocratic, or a mixture of both democratic and autocratic networks [49–51,53,54]. In this context we investigated the chemical noise propagation in an autocratic network in which the nodes in a particular layer regulate the nodes in the layer below. Our objective was to establish the role of the qualitative (activatory/inhibitory) and quantitative (strength) nature of regulatory interactions in dictating the variability in the autocratic network. We used the mass action rate law of chemical reaction to model the network such that we can use the stochastic simulation algorithm [57] to accurately estimate the intrinsic chemical noise in the network.

We determined that the steady state statistical properties of the output node are regulated strongly by the qualitative nature of the proximal (direct) and near-nonproximal (indirect) interactions. Whereas the far-nonproximal regulations do not influence such properties significantly. Our calculations reveal that the noise passes through a minimum as a function of the average abundance, particularly when the network consists of more activatory near-nonproximal regulations than the inhibitory near-nonproximal regulations. The consequence of this scaling is that the variability of the output node is large both in the low and high abundance regimes. This scaling of noise with the average is unconventional in a sense that the system exhibits more variability even though the average is large. We showed that the nontrivial scaling of noise with the average was due to the bursty kinetics of the system under the regulatory influence of a large number of direct activatory interactions from the nodes in the adjacent layer. By varying the strengths of activatory and inhibitory interactions, we show that the increased strength of activatory regulation promotes the nontrivial scaling of the variability. We demonstrate that the activatory regulations either in number or in strength cause increased variability in the system by producing bursty trajectories. We also find that the qualitative nature of scaling remain intact with the introduction of democratic mutual interactions among nodes in a particular layer. We have previously investigated regulation of chemical noise in a purely democratic network and we showed a biphasic scaling of noise [59]. In contrast to the purely democratic network, the fully autocratic and mixed networks both exhibit a nontrivial scaling of noise in which the downstream node becomes noisy both in the low and high abundance regimes.

ACKNOWLEDGMENTS

The work was supported by funding from the Science and Engineering Research Board, Department of Science and Technology (India), Grant No. EMR/2015/001899, to D.B. S.D. acknowledges fellowship from INSPIRE program of Department of Science and Technology, India.

[1] E. M. Ozbudak, M. Thattai, I. Kurtser, A. D. Grossman, and A. van Oudenaarden, Nat. Genet. **31**, 69 (2002).

[2] M. B. Elowitz, A. J. Levine, E. D. Siggia, and P. S. Swain, Science **297**, 1183 (2002).

[3] W. J. Blake, M. Kærn, C. R. Cantor, and J. J. Collins, Nature (London) **422**, 633 (2003).
[4] J. M. Raser and E. K. O'Shea, Science **304**, 1811 (2004).
[5] S. D. Talia, J. M. Skotheim, J. M. Bean, E. D. Siggia, and F. R. Cross, Nature (London) **448**, 947 (2007).
[6] N. Geva-Zatorsky, N. Rosenfeld, S. Itzkovitz, R. Milo, A. Sigal, E. Dekel, T. Yarnitzky, Y. Liron, P. Polak, G. Lahav, and U. Alon, Mol. Syst. Biol. **2**, 2006.0033 (2006).
[7] S. L. Spencer, S. Gaudet, J. G. Albeck, J. M. Burke, and P. K. Sorger, Nature (London) **459**, 428 (2009).
[8] O. Feinerman, J. Veiga, J. R. Dorfman, R. N. Germain, and G. Altan-Bonnet, Science **321**, 1081 (2008).
[9] A. A. Cohen, N. Geva-Zatorsky, E. Eden, M. Frenkel-Morgenstern, I. Issaeva, A. Sigal, R. Milo, C. Cohen-Saidon, Y. Liron, Z. Kam, L. Cohen, T. Danon, N. Perzov, and U. Alon, Science **322**, 1511 (2008).
[10] A. Raj and A. van Oudenaarden, Cell **135**, 216 (2008).
[11] A. Sanchez, S. Choubey, and J. Kondev, Annu. Rev. Biophys. **42**, 469 (2013).
[12] A. Eldar and M. B. Elowitz, Nature (London) **467**, 167 (2010).
[13] G. Balázsi, A. van Oudenaarden, and J. J. Collins, Cell **144**, 910 (2011).
[14] T. Hagai, X. Chen, R. J. Miragaia, R. Rostom, T. Gomes, N. Kunowska, J. Henriksson, J.-E. Park, V. Proserpio, G. Donati, L. Bossini-Castillo, F. A. V. Braga, G. Naamati, J. Fletcher, E. Stephenson, P. Vegh, G. Trynka, I. Kondova, M. Dennis, M. Haniffa, A. Nourmohammad, M. Laessig, and S. A. Teichmann, Nature (London) **563**, 197 (2018).
[15] L. S. Weinberger, J. C. Burnett, J. E. Toettcher, A. P. Arkin, and D. V. Schaffer, Cell **122**, 169 (2005).
[16] M. Acar, J. T. Mettetal, and A. van Oudenaarden, Nat. Genet. **40**, 471 (2008).
[17] T. Çağatay, M. Turcotte, M. B. Elowitz, J. Garcia-Ojalvo, and G. M. Süel, Cell **139**, 512 (2009).
[18] M. Thattai and A. van Oudenaarden, Proc. Natl. Acad. Sci. USA **98**, 8614 (2001).
[19] J. Paulsson, Nature (London) **427**, 415 (2004).
[20] J. Pedraza and A. van Oudenaarden, Science **307**, 1965 (2005).
[21] N. Friedman, L. Cai, and X. S. Xie, Phys. Rev. Lett. **97**, 168302 (2006).
[22] V. Shahrezaei and P. S. Swain, Proc. Natl. Acad. Sci. **105**, 17256 (2008).
[23] J. M. Pedraza and J. Paulsson, Science **319**, 339 (2008).
[24] T. Jia and R. V. Kulkarni, Phys. Rev. Lett. **106**, 058102 (2011).
[25] J. Paulsson, Phys. Life Rev. **2**, 157 (2005).
[26] I. Tirosh and N. Barkai, Genome Res. **18**, 1084 (2008).
[27] L. Bai, G. Charvin, E. D. Siggia, and F. R. Cross, Developmental Cell **18**, 544 (2010).
[28] D. Nicolas, B. Zoller, D. M. Suter, and F. Naef, Proc. Natl. Acad. Sci. **115**, 7153 (2018).
[29] J. M. G. Vilar and L. Saiz, Phys. Rev. E **89**, 062703 (2014).
[30] G. Hornung, R. Bar-Ziv, D. Rosin, N. Tokuriki, D. S. Tawfik, M. Oren, and N. Barkai, Genome Res. **22**, 2409 (2012).
[31] K. Murphy, R. Adams, X. Wang, G. Balázsi, and J. Collins, Nucleic Acids Res. **38**, 2712 (2010).
[32] T.-L. To and N. Maheshri, Science **327**, 1142 (2010).
[33] A. Sanchez, H. G. Garcia, D. Jones, R. Phillips, and J. Kondev, PLoS Comput. Biol. **7**, e1001100 (2011).
[34] L. B. Carey, D. van Dijk, P. M. A. Sloot, J. A. Kaandorp, and E. Segal, PLoS Biol. **11**, e1001528 (2013).
[35] D. L. Jones, R. C. Brewster, and R. Phillips, Science **346**, 1533 (2014).
[36] D. Das, S. Dey, R. C. Brewster, and S. Choubey, PLoS Comput. Biol. **13**, e1005491 (2017).
[37] A. Becskei and L. Serrano, Nature (London) **405**, 590 (2000).
[38] M. Hinczewski and D. Thirumalai, J. Phys. Chem. B **120**, 6166 (2016).
[39] M. Thattai and A. van Oudenaarden, Biophys. J. **82**, 2943 (2002).
[40] S. Hooshangi, S. Thiberge, and R. Weiss, Proc. Natl. Acad. Sci. **102**, 3581 (2005).
[41] O. Brandman, J. E. Ferrell, R. Li, and T. Meyer, Science **310**, 496 (2005).
[42] R. Maithreye and S. Sinha, Physical Biol. **4**, 48 (2007).
[43] H. Zhang, Y. Chen, and Y. Chen, PLOS ONE **7**, e51840 (2012).
[44] M. S. Avendaño, C. Leidy, and J. M. Pedraza, Nat. Commun. **4**, 2605 (2013).
[45] S. Chepyala, Y.-C. Chen, C.-C. Yan, C.-Y. Lu, Y.-C. Wu, and C.-P. Hsu, Sci. Rep. **6**, 23607 (2016).
[46] C. Briat, A. Gupta, and M. Khammash, Cell Systems **2**, 15 (2016).
[47] A. Dey and D. Barik, PLOS ONE **12**, e0188623 (2017).
[48] S. Das and D. Barik, Phys. Rev. E **100**, 052402 (2019).
[49] H.-W. Ma, J. Buer, and A.-P. Zeng, BMC Bioinf. **5**, 199 (2004).
[50] H. Yu and M. Gerstein, Proc. Natl. Acad. Sci. **103**, 14724 (2006).
[51] R. Jothi, S. Balaji, A. Wuster, J. A. Grochow, J. Gsponer, T. M. Przytycka, L. Aravind, and M. M. Babu, Mol. Syst. Biol. **5**, 294 (2009).
[52] Y. Bar-Yam, D. Harmon, and B. de Bivort, Science **323**, 1016 (2009).
[53] N. Bhardwaj, K.-K. Yan, and M. B. Gerstein, Proc. Natl. Acad. Sci. **107**, 6841 (2010).
[54] D. Abd-Rabbo and S. Michnick, BMC Syst. Biol. **11**, 38 (2017).
[55] A. Belle, A. Tanay, L. Bitincka, R. Shamir, and E. K. O'Shea, Proc. Natl. Acad. Sci. **103**, 13004 (2006).
[56] S. B. Cambridge, F. Gnad, C. Nguyen, J. L. Bermejo, M. Krüger, and M. Mann, J. Proteome Res. **10**, 5275 (2011).
[57] D. T. Gillespie, J. Comput. Phys. **22**, 403 (1976).
[58] O. Martin, A. Krzywicki, and M. Zagorski, Phys. Life Rev. **17**, 124 (2016).
[59] S. Das and D. Barik, Phys. Rev. E **101**, 042407 (2020).
[60] D. Barik, D. A. Ball, J. Peccoud, and J. J. Tyson, PLoS Comput. Biol. **12**, e1005230 (2016).
[61] D. Barik, W. T. Baumann, M. R. Paul, B. Novak, and J. J. Tyson, Mol. Syst. Biol. **6**, 405 (2010).